Published in final edited form as:

Biochemistry. 2018 April 10; 57(14): 2140–2149. doi:10.1021/acs.biochem.8b00150.

Quantitative Characterization of Bivalent Probes for a Dual Bromodomain Protein, Transcription Initiation Factor TFIID Subunit 1

Junghyun L. Suh[†], **Brian Watts**[‡], **Jacob I. Stuckey**[†,§], **Jacqueline L. Norris-Drouin**[†], **Stephanie H. Cholensky**[†], **Bradley M Dickson**[†,||], **Yi An**[†], **Sebastian Mathea**[⊥,▼], **Eidarus Salah**[⊥], **Stefan Knapp**[⊥,□], **Abid Khan**[#], **Alexander T. Adams**[#], **Brian D. Strahl**[#], **Cari A. Sagum**[¶], **Mark T. Bedford**[¶], **Lindsey I. James**[†], **Dmitri B. Kireev**[*,†], and **Stephen V. Frye**[*,†]

[†]Center for Integrative Chemical Biology and Drug Discovery, Division of Chemical Biology and Medicinal Chemistry, UNC Eshelman School of Pharmacy, University of North Carolina at Chapel Hill, Chapel Hill, North Carolina 27599, United States

[‡]Duke Human Vaccine Institute, Duke University School of Medicine, Duke University, Durham, North Carolina 27710, United States

[§]Constellation Pharmaceuticals, 215 First Street, Suite 200, Cambridge, Massachusetts 02141, United States

[||]Center for Epigenetics, Van Andel Research Institute, Grand Rapids, Michigan 49503, United States

[⊥]Nuffield Department of Medicine, Structural Genomics Consortium, Old Road Campus Research Building, Oxford University, Oxford, OX3 7DQ, United Kingdom

[#]Department of Biochemistry and Biophysics and Lineberger Comprehensive Cancer Center, University of North Carolina School of Medicine, Chapel Hill, North Carolina 27599, United States

[¶]Department of Epigenetics and Molecular Carcinogenesis, University of Texas MD Anderson Cancer Center, Smithville, Texas 78957, United States

[□]Institute of Pharmaceutical Chemistry and Buchmann Institute for Life Sciences (BMLS), Structure Genomics Consortium, Goethe-University Frankfurt, Max von Lauestrasse 9, 60438 Frankfurt am Main, Germany

[▼]German Cancer Centre (DKFZ), DKTK Consortium, 60438 Frankfurt am Main, Germany

[*]Corresponding Authors: dmitri.kireev@unc.edu. Phone: 919-843-8457. svfrye@email.unc.edu. Phone: 919-843-5486.

ORCID

Junghyun L. Suh: 0000-0003-0508-6491
Bradley M Dickson: 0000-0002-4995-9111
Lindsey I. James: 0000-0002-6034-7116
Stephen V. Frye: 0000-0002-2415-2215

Notes

The authors declare no competing financial interest.

ASSOCIATED CONTENT

Supporting Information

The Supporting Information is available free of charge on the ACS Publications website at DOI: 10.1021/acs.bio-chem.8b00150. Supporting figures, tables, synthetic schemes, a detailed description of the chemical synthesis and characterization, and the materials and experimental methods (PDF)

Abstract

Multivalent binding is an efficient means to enhance the affinity and specificity of chemical probes targeting multidomain proteins in order to study their function and role in disease. While the theory of multivalent binding is straightforward, physical and structural characterization of bivalent binding encounters multiple technical difficulties. We present a case study where a combination of experimental techniques and computational simulations was used to comprehensively characterize the binding and structure–affinity relationships for a series of Bromosporine-based bivalent bromodo-main ligands with a bivalent protein, Transcription Initiation Factor TFIID subunit 1 (**TAF1**). Experimental techniques—Isothermal Titration Calorimetry, X-ray Crystallography, Circular Dichroism, Size Exclusion Chromatography-Multi-Angle Light Scattering, and Surface Plasmon Resonance—were used to determine structures, binding affinities, and kinetics of monovalent ligands and bivalent ligands with varying linker lengths. The experimental data for monomeric ligands were fed into explicit computational simulations, in which both ligand and protein species were present in a broad range of concentrations, and in up to a 100 s time regime, to match experimental conditions. These simulations provided accurate estimates for apparent affinities (in good agreement with experimental data), individual dissociation microconstants and other microscopic details for each type of protein–ligand complex. We conclude that the expected efficiency of bivalent ligands in a cellular context is difficult to estimate by a single technique *in vitro*, due to higher order associations favored at the concentrations used, and other complicating processes. Rather, a combination of structural, biophysical, and computational approaches should be utilized to estimate and characterize multivalent interactions.

Graphical Abstract

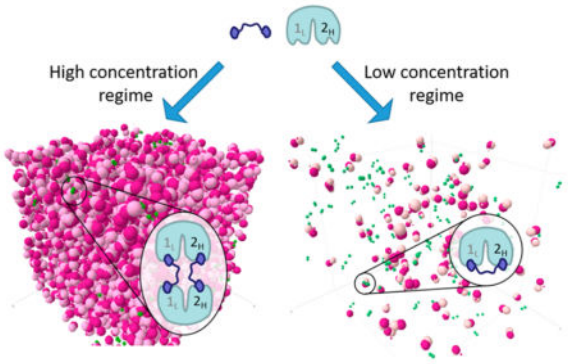

A protein–ligand complex features multiple simultaneous, independent, noncovalent interactions. In the case of bivalent binding, a ligand composed of two linked monomeric units binds cooperatively to two structural domains within a single protein. In general, the bivalent ligand is expected to demonstrate a significant gain in binding affinity as compared to either monovalent ligand.[1] This affinity enhancement effect is critical in biology where individual protein–protein contacts are often weak, and has been exploited in multiple practical applications including nanomedicine and material sciences.[2–4] In chemical biology, multivalent binding can potentially be used to enhance both the affinity and specificity of chemical probes to create useful tools to study the function of proteins and their roles in

disease.[5,6] Indeed, a monovalent probe may bind not only a structural domain of a protein of interest, but also a large number of structurally related domains. In contrast, bivalent probes have the potential to demonstrate far better selectivity by engaging two structural domains that are unlikely to exist in the same spatial orientation in more than one protein, creating a unique binding site. Additionally, bivalent probes can lead to significant affinity enhancements when proteins are known to exist as dimers or polyvalent complexes.[7] The field of chromatin biology and epigenetics has been accelerated by the development of chemical probes as there has been a concerted, prospective effort to discover these tools.[8] The concept of multivalency in chromatin regulation has been well recognized, as many of the proteins involved contain multiple ligandable domains and/or exist within complexes that assemble multiple binding sites.[9] Accordingly, bivalent ligand discovery to generate chromatin-targeted chemical probes has been exemplified by bivalent BRD4 inhibitors (BRD4 features two BET-family bromodomains) showing significant enhancement in functional in vivo activity compared to the constituent monomeric ligands.[10,11]

Here, we present a case study where a combination of experimental techniques and computational simulations were used to comprehensively characterize the binding and structure-affinity relationships for a series of bivalent ligands and the bivalent protein, Transcription Initiation Factor TFIID subunit 1 (TAF1). TAF1 is the largest component and core scaffold of the TFIID basal transcription factor complex and is essential for progression of the G1 phase of the cell cycle.[12] TAF1 contains N- and C-terminal Ser/Thr kinase domains which can autophosphorylate or trans-phosphorylate other transcription factors, while also possessing DNA-binding activity. It promotes euchromatinization through propagation of H3 and H4 histone acetylation marks[12] and contains a pair of closely related (43% sequence identity) bromodomains. The dual TAF1 bromodomains have been shown to bind a broad range of polyacetylated histone peptides with micromolar affinity, and the corresponding nonacetylated peptides with significantly lower affinity.[13] Importantly, there is evidence of a multivalent affinity enhancement when comparing singly to doubly acetylated histone peptides, resulting in a 7-fold enhancement in K_d.[13]

In the design of TAF1 bivalent ligands, we utilized a previously published pan-bromodomain probe, Bromosporine (BSP).[14] BSP possesses nanomolar affinity for bromodomain 2 (BD2) of TAF1 and significantly weaker (micromolar) affinity for bromodomain 1 (BD1).[14] If we limit our analysis of TAF1 and BSP-based bivalent ligands to complexes with stoichiometries up to 2:2, 13 distinct binding modes are theoretically possible (see Supporting Information (SI) Figure S1 for a comprehensive depiction of possible complexes). However, in order to simplify discussion, we will focus on the 6 bivalent complexes that preferentially ligate the high affinity site of TAF1 (BD2), before engaging the low affinity site (BD1) (Figure 1), with only one corresponding to typical expectations for multivalent engagement (Figure 1c). We utilized Isothermal Titration Calorimetry (ITC), X-ray Crystallography, Circular Dichroism (CD), Size Exclusion Chromatography-Multi-Angle Light Scattering (SEC-MALS), and Surface Plasmon Resonance (SPR) to determine structures, binding affinities, and kinetics of monomeric ligands, as well as apparent affinities for bivalent ligands with varying linker lengths to the TAF1 tandem bromodomain. The resulting experimental data for monomeric units were fed into explicit computational simulations, in which ligand and protein species were represented in a broad range of

concentrations and in up to a 100 s time regime, matching experimental conditions. These simulations provided accurate estimates for apparent affinities (in good agreement with experimental data) and individual dissociation microconstants and other microscopic details for each type of protein–ligand complex.

While the effect of binding enhancement for bivalent ligands has been theoretically characterized from the first principles of thermodynamics and statistical physics,[15–18] we found that the physical and structural characterization of bivalent binding encounters multiple technical difficulties. In particular, both the bivalent ligand and protein generally have flexible linkers between the monomeric ligands or individual binding modules, respectively, making them difficult to study by X-ray crystallography and Nuclear Magnetic Resonance (NMR). Moreover, the multitude of available binding modes can confound the analysis of biophysical data, especially at high protein concentrations required for techniques such as ITC. Our results using TAF1 as a prototypical example suggest that many prior reports of *in vitro* bivalent affinity enhancements have overlooked the multiple modes of bivalent enhancement actually prevalent in experimental systems (Figure 1).

MATERIALS AND METHODS

ITC Experiments

All ITC measurements were recorded at 25 °C using an AutoITC200 microcalorimeter (MicroCal Inc., MA). Protein stocks were prepared in ITC buffer (25 mM Tris-HCl, pH 8, 150 mM NaCl, and 2 mM β-mercaptoethanol) and then diluted into ITC buffer to achieve a final concentration of 25 μM (325 μL). Bromosporine was dissolved in DMSO to a stock concentration of 10 mM and then diluted to a final concentration of 500 μM. Other compounds dissolved in water to a stock concentration of 10 mM and diluted to a final concentration of 500 μM for **1** (UNC4493) and **5** (UNC4494) and 250 μM for bivalent ligands. The concentration of the protein stock solution was established using the Edelhoch method, whereas compound stock solutions were prepared based on mass. A typical experiment included a single 0.2 μL compound injection into a 200 μL cell filled with protein, followed by 26 subsequent 1.5 μL injections of compound. Injections were performed with a spacing of 180 s and a reference power of 8 μcal/s. The titration data was analyzed using Origin Software (MicroCal Inc., USA) by nonlinear least-squares, fitting the heats of binding as a function of the compound:protein ratio to a one-site binding model. The first data point was deleted from all analyses. All assays were run in triplicate. The data was fit separately for each experiment and the reported K_d is the average of the three runs. Error was calculated as the standard deviation of the three K_d values.

Molecular Dynamics

Molecular dynamics (MD) were performed using GROMACS 4.6.3 software suite[19] with Charmm27 force field.[20] The force field parameters of substrates (IP7, IP8) and cofactors (ADP, ATP) were obtained from SwissParam.[21] For each simulation, the PPIP5K2-ligand complex was dissolved in a 10 nm × 10 nm × 7 nm rectangular box. The box was filled with TIP3P water[22] and ions were neutralized by Na^+ and Cl^-. Each dissolved system was first energy minimized by steepest descent algorithm, then equilibrated in two stages. First a 500

ps constant NVT equilibration was performed to allow water molecules to fill vacancies in protein; then a 2 ns constant NPT equilibration was performed to remove bad contacts and interactions. For each dissolved system, constant NVT simulations were performed for 1 μs. In the simulation, the force was calculated every 2 fs while the coordinates were saved every 20 ps. LINCS[23] was applied to restrain bonds, Particle Mesh Ewald (PME) was applied for long-range electrostatics interactions,[24] modified Berendsen thermostat[25] was used for temperature coupling, and periodic boundary condition was applied to eliminated image effects.

SEC-MALS Experiments

Protein stocks were prepared in ITC buffer (25 mM Tris-HCl, pH 8, 150 mM NaCl, and 2 mM β-mercaptoethanol) and then diluted in 25 mM Tris-HCl, pH 8, 150 mM NaCl, 1 mg/mL BSA, and 0.005% Tween20 to achieve a final concentration of 25 μM for initial studies and 20 μM for titration studies. The final concentration of compounds was adjusted to compound:protein molar ratios of 4:1 for **1** (UNC4493) and **5** (UNC4494) and 2:1 for bivalent ligands. For the titration studies, compound:protein molar ratios of 1:4, 1:2, 1:1, and 2:1 were chosen. 100 μL of each sample was loaded sequentially onto a Superdex 200 size exclusion column (24 mL) pre-equilibrated with buffer (25 mM Tris-HCl, pH 8, 150 mM NaCl, 1 mg/mL BSA, and 0.005% Tween20). The eluted samples first passed through a Wyatt multiangle light scattering system (DAWN HELEOS-II) and then a Wyatt Trex refractometer. The data were analyzed using ASTRA v 6 software (Wyatt Technology, Santa Barbara, CA).

SPR Experiments

The binding kinetics of protein–small molecule interactions were assessed by surface plasmon resonance (SPR) on a Biacore T200 at 25 °C in TBS running buffer (25 mM Tris-HCl, 150 mM NaCl, pH 8.0). Covalent immobilization of TAF1-WT, TAF1-N1460D, and TAF1-N1583D proteins to an NTA-modified carboxymethyldextran sensor surface was performed via simultaneous His-capture and amine coupling chemistry at a flow rate of 10 μL/min. The NTA sensor surfaces were loaded with 0.5 mM $NiCl_2$ for 60 s and activated by a 7 min injection of a solution of 50 mM *N*-hydrosuccinimide (NHS) and 200 mM 1-ethyl-3-(3-(dimethylamino)propyl) carbodiimide hydrochloride (EDC). Protein ligand solutions (200 nM in TBS) were injected over the surfaces (60–720 s) to achieve the desired immobilization levels [N1460D: 640 RU, N1583D: 1000 RU, WT: 440 RU (25 °C); N1460D: 620 RU, N1583D: 780 RU, WT: 570 RU (15 °C)], and the surfaces were deactivated with a 12 min injection of 1 M ethanolamine hydrochloride-NaOH, pH 8.5. Kinetic evaluation was performed by sequential 3 min injections of varying concentrations (0.05–50 μM) of **5** (UNC4494), **2** (UNC4495), **3** (UNC4512), and **4** (UNC4928) at either 25 or 15 °C, followed by a 7 min dissociation phase at a flow rate of 30 μL/min (25 °C) or 50 μL/min (15 °C). Surfaces were regenerated between small molecule analyte injections with a 30 s injection of 75% (25 °C) or 50% (15 °C) ethylene glycol. Data analysis and curve fitting was performed with the Biacore T200 Evaluation Software (v 2.0) using the heterogeneous ligand model which interprets the observed binding as the sum of two kinetic regimes and allows for differentiation of fast and slow kinetic components in biphasic

curves. Experiments were performed in duplicate and reported values are the averages and the standard and propagated errors for kinetic and affinity constants, respectively.

Brownian Dynamics

Coarse-grained simulations were performed using a custom Matlab script. Molecules were represented as objects, each composed of one or more objects or particles. Objects of two types, chains and bodies, were used in this study. TAF1 dual bromodomain protein was modeled as a chain of two bodies. The diffusion of a body that is a node in a chain is constrained by tethers to the adjacent objects in the chain. The random vector **r** pointing to the next position of an object in a chain would be damped by a multiplier $\lambda(d) = \begin{cases} 1, & d < \bar{d} \\ e^{-\omega(d-\bar{d})}, & \bar{d} < d < d_{max} \\ 0, & d > d_{max} \end{cases}$, where d is the distance between the linked objects, $\bar{d}$ is a mean end-to-end distance for the linker polymer, d_{max} is a largest distance allowed (it slightly exceeds the physical length of a fully stretched linker), and ω is a coefficient adjusted so that $\lambda(d)$ would almost vanish for $d = d_{max}$. Here, $\lambda(d)$ was designed so that the probability density function (PDF) for domain–domain distances would mimic, in a speed-efficient way, an end-to-end PDF for an ideal polymer. For the bromo–bromo linker of TAF1, d_{max} was set to 4 nm, and $\bar{d}$ to 3.5 nm. The bromodomain body was composed of a 'bromo_core' and a 'bromo_pocket' particle, hard spheres with respective radii of 1.5 and 0.3 nm. The bivalent BSP-based ligand was modeled as a chain of two "BSP" particles (with a radius of 0.3 nm). BSP–BSP linkers were represented as described above for the bromo–bromo linker in the TAF1 model. For compounds **2** (PEG4), **3** (PEG17), and **4** (PEG29), d_{max} was set to, respectively, 2.4, 8, and 12 nm and $\bar{d}$ to 1.1, 1.7, and 2 nm.

The simulation engine recalculates the coordinates for each object at discrete time steps and performs chemical reactions (including complex formation) for particles satisfying the reaction conditions. Given the time/space granularity for the system of interest, overdamped Langevin dynamics with isotropic diffusion (also called Brownian dynamics) provides a relevant framework.[26] The coordinates of the particles (**x**) for the next time step ($t + \mathrm{d}t$) are updated according to

$$\frac{d\mathbf{x}}{\mathrm{d}t} = -\frac{\nabla V(\mathbf{x})}{m} + \frac{(2\gamma k_B T)^{1/2} R(t)}{m}$$

where the first term is determined by the gradient of the potential V resulting from the force field (there were no interaction potentials in the current study). The second term, determined by the stationary Gaussian process $R(t)$ responsible for random displacements with magnitudes controlled by the damping constant γ, tuned based on available experimental data on molecular diffusion in cells.[27,28] Time step was set to 1 μs and velocity for a single particle of a radius of 0.35 nm (that is, a single bromodomain) was set to 2 nm.

RESULTS AND DISCUSSION

Design, Synthesis, and Characterization of Monovalent TAF1 Binders

We first sought to design and characterize a monovalent BSP-based ligand which would serve as an appropriate reference to investigate the affinity gain for the corresponding bivalent derivatives. BSP was synthesized following a previously reported route with slight modifications[14] (see SI Scheme S1). Its binding to recombinant TAF1 protein, prepared from a construct containing the isolated dual bromodomains (TAF1 **BD1**–**BD2**), was characterized by ITC resulting in an apparent K_d of 320 ± 50 nM and stoichiometry of 1:2 TAF1:BSP with a monophasic binding isotherm, thus suggesting engagement of both bromodomains by BSP (see SI Figure S2).

Next, in order to build bivalent molecules, a linker attachment site needed to be identified that was synthetically accessible and unlikely to perturb ligand binding. Using a model of BSP-bound TAF1, built using the X-ray structure of the BSP:BRPF1 complex (PDB: 5C7N[29]) as a structural template, we hypothesized that the ethyl carbamate moiety was largely solvent exposed and would be an appropriate site for functionalization. UNC4493 (**1**) (Figure 2a,b and SI Scheme S2) was designed and synthesized as a compound with high aqueous solubility, a functionalizable group for linker attachment, and binding affinity to TAF1 comparable to that of BSP (K_d = 300 ± 47 nM, N = 2.0 ± 0.2) (Figure 2c). Due to the structural differences between **BD1** and **BD2** and differences in binding of BSP for each domain, we sought to determine the affinity of **1** for each bromodomain. To do so, we utilized docking models of **1** in complex with both **BD1** and **BD2** to identify site-directed mutants aimed at crippling the binding function of each BD. According to the models and the experimental structure of the BSP complex with TAF1L(2),[14] the conserved asparagine residues that are also required for binding to acetyl-lysines in most bromodomains, Asn1460 and Asn1583 are key residues for ligand binding to **BD1** and **BD2**, respectively, and therefore we prepared two TAF1 mutants, N1460D and N1583D. Importantly, it was previously reported that a dual N1460D/N1583D TAF1 mutant maintained its structural integrity while losing binding to acetylated p53, a cognate TAF1 binder.[13,30] Circular dichroism was used to compare the secondary structures of wild-type and mutant TAF1, and the data indicated that these point mutants have a negligible effect on the overall secondary structure of the TAF1 bromodomains (SI Figure S3). In ITC experiments, compound **1** bound TAF1-N1460D where **BD1** is inactivated with a K_d of 93 ± 35 nM and TAF1-N1583D where **BD2** is inactivated with a K_d of 2350 ± 470 nM (SI Figure S4). These results demonstrate that compound **1** binds **BD2** about 25-fold more potently than **BD1** and are consistent with previously published data on BSP binding to isolated TAF1 **BD1** (low affinity site) and **BD2** (high affinity site).[14]

Design, Synthesis, and Characterization of Bivalent TAF1 Binders

There are two putative causes of the affinity enhancement that can result from bivalent binding. The first is a local concentration effect, as a momentarily unbound monomeric unit of a bivalently bound ligand will more rapidly rebind the target because it is not free to leave the protein's vicinity (the mean *rebinding* time here is inversely proportional to association rate constant k_{on}; hence shorter time results in lower K_d, according to $K_d = k_{off}/k_{on}$). The

effective concentration of the monomer in the vicinity of the unoccupied protein binding site can be written as

$$C_e = 1/V_a \quad (1)$$

where $V_a = V_l - V_e$ is the total volume available for one monomer while the other remains protein-bound; $V_l = 4/3\pi l^3$ is the volume potentially available to one monomeric unit while the other one is fixed; l is the length of a fully stretched linker between the two monomeric units; and V_e is the excluded volume, that is, the bulk of the protein, which for short linkers or deeply buried binding pockets might be more than a half of V_l (note that eq 1 is only exact for an ideal linker with a uniform end-to-end distance distribution, but is a reasonable approximation in this case). For example, the effective concentration of a monomeric unit within a bivalent molecule containing a linker of l = 20 Å would be 0.28 M, which is 3–8 orders of magnitude higher than a typical ligand concentration in a biophysical experiment. Therefore, in a typical experimental setting involving multivalent binding, the contribution of *rebinding* to the affinity gain would be dominant, and would only depend on the linker length of the ligand as opposed to the protein concentration. Second, a bivalent ligand can simultaneously bind two proteins (Figure 1f–h) intermolecularly and result in a significant gain in affinity. This contribution fully depends on the probability of an encounter between a ligand-bound protein and a free protein, which in turn is determined by the ligand and protein concentrations.

To quantify the respective contributions of intramolecular *rebinding* and intermolecular *biprotein binding* to the affinity of BSP-based bivalent ligands for TAF1, the effect of varying the linker length needs to be considered. Polyethylene glycol (PEG) has been chosen as a linker unit because it aids solubility and its behavior closely mimics that of an ideal polymer chain.[31] We first sought to determine the shortest possible linker that would allow both connected monomers to simultaneously bind to **BD1** and **BD2** of a single TAF1 protein. Based on the X-ray structure of the apo-TAF1 double BD module (PDB: 1EQF),[13,32] a PEG_4 linker appeared to be long enough to allow a bivalent interaction (Figure 3a), although this would require a fully extended linker which may in turn impose a significant entropic penalty on binding. We further used all-atom molecular dynamics (MD) simulations to assess the configurational space accessible to a protein-bound ligand. The MD trajectory, as reflected by its visual representation (Figure 3b) and the probability density distribution function of the ligand root-mean-square distance (RMSD) to the initial docking pose (SI Figure S5), displays a significant freedom of motion within TAF1. This freedom is in part due to minor **BD1** and **BD2** rearrangements, but also because of ligand monomer motions within their respective binding pockets. As this freedom of motion should compensate for entropic penalties of binding, PEG_4 was selected as the shortest linker for our series of bivalent ligands. Two other linkers, PEG_{17} and PEG_{29}, were also chosen as they differ substantially in length from PEG_4 and each other to enable observable differences in the rebinding effect and hence overall TAF1 affinity. Respective bivalent compounds **2** (UNC4495), **3** (UNC4512), and **4** (UNC4928) (Figure 3a and SI Scheme S3) were synthesized and their binding affinities determined by ITC (Figure 3c). A monovalent ligand

—compound **5** (UNC4494) with a PEG_4 linker attached (Figure 3a)—was also synthesized as a control. Importantly, evaluating the affinity of **5** enables determination of whether the linker itself may contribute to ligand affinity. The binding affinity of compound **5** for TAF1 was somewhat weaker than compound **1** (Figure 3c), confirming that the presence of the PEG linker did not itself enhance binding.

Overall, ITC results for bivalent ligands **2**–**4** showed a consistent and significant affinity gain (60- to 100-fold) in each case over the monovalent reference compound **5** (Figure 3c). However, the observed stoichiometries were not the same for all three bivalent systems. While compounds **2** and **3** displayed a prevalence of 1:1 TAF1:BSP stoichiometry, the data for ligand **4** with the longest PEG linker suggests a ratio of 2:1 TAF1:BSP. In a system such as this involving a bivalent ligand and a bivalent protein with heterogeneous monomeric units as well as experimental conditions that require extremely high concentrations, multiple types of complexes may potentially exist (Figure 1 and SI Figure S1), significantly complicating simplistic assumptions of anticipated stoichiometry. In particular, the probability of ligands binding more than one protein (Figure 1f–h) is especially high in the beginning of the ligand titration, at the highest free protein concentrations. Consequently, the best-fit stoichiometry values may obfuscate a significantly more complex reality. For the same reason, it is difficult to definitively rationalize whether the variation of apparent ITC affinity values reflect the linker's role in the *rebinding* effect. Therefore, we proceeded with an array of structural and biophysical studies to more thoroughly and systematically evaluate the microscopic details of the bivalent protein–ligand interactions.

Biophysical Characterization of Bivalent Binders

X-ray Crystallography—We first sought direct evidence of bivalent complexes, either 1:1 (protein:ligand) (Figure 1c,d), 1:2 (Figure 1e), 2:1 (Figure 1f), or 2:2 (Figure 1g,h), in cocrystallization studies. Although a cocrystal structure of a TAF1-bound compound **3** (PEG_{17}) was solved (Figure 4a) and the asymmetric unit displays both **BD1** and **BD2** pockets occupied by ligand monomers, no electron density corresponding to the PEG chain was observed, likely due to its flexibility. This outcome, while directly confirming simultaneous ligand binding to both TAF1 bromodomains, does not provide any direct information regarding which protein–ligand complex might be prevalent (at least, under crystallization conditions) or the binding stoichiometry. Nevertheless, this structural analysis was useful to corroborate the previously developed docking models of BSP binding. In particular, it confirms that monomeric BSP units adopt similar binding modes in both **BD1** and **BD2** featuring direct hydrogen bonds with N1460 (**BD1**) and N1583 (**BD2**) and indirect hydrogen bonds, via water molecules, with Y1417 (**BD1**) and Y1540 (**BD2**). Importantly, this first liganded **BD1** structure also provides a sound explanation for why **BD2** is a higher affinity BSP binder than **BD1**. In **BD2**, the side chain of Tyr1589 forms highly favorable aromatic stacking interactions with the triazolopyridazine ring of the BSP unit, whereas in **BD1**, the respective residue is Leu1466, which is unable to stabilize ligand binding to the same extent.

SEC-MALS—We next examined the interactions between our bivalent ligands and TAF1 by SEC-MALS which provides an effective means to determine molecular weights of

proteins or protein assemblies and, consequently, deduce stoichiometry of any complex present.[33] We applied SEC-MALS to detect the presence of TAF1 dimers in solution, as well as the dependence of TAF1 dimerization on ligand concentration. In the absence of ligand, TAF1 is mostly present as a monomer, and TAF1 remains monomeric in the presence of monovalent ligands **1** and **5**. In contrast, the addition of any of the bivalent ligands **2**–**4** caused almost complete dimerization of TAF1 (Figure 4b and SI Table S1). Moreover, when compound **3** was titrated into TAF1, the extent of TAF1 dimerization increased in a dose-dependent manner, confirming that dimerization is ligand induced (SI Figure S6 and SI Table S2). Combining (i) the low dimerization propensity of TAF1 bromodomains and (ii) the fact that the X-ray structure did not reveal any ligand-induced structural rearrangements, it would be reasonable to expect that the ligand-mediated dimerization does not involve any cooperative effect of direct **BD1**–**BD2** binding. More generally, these results suggest that the composition of solutions containing bivalent ligand and protein may be complex and concentration-dependent and emphasize the need for a technique that would help to rule out the presence of 1:2 (Figure 1e) or 2:1 (Figure 1f) TAF1:ligand complexes.

SPR—SPR is a label-free, surface-based technology commonly used to study protein–ligand interactions in which a soluble ligand is injected across a protein-functionalized sensor surface. Importantly, protein surface densities can be controlled such that the possibility of the formation of complexes with stoichiometries higher than 1:1 is greatly reduced as the proteins are unable to dimerize once functionalized to the surface. This distinguishes SPR from the other experimental techniques discussed above. The assay readout is monitored in real time and affords direct assessment of the association and dissociation rate constants (k_a and k_d), and thus the binding affinity (K_d). Assessment of TAF1 binding kinetics and affinity for the bivalent ligands **2**–**4** required careful surface functionalization and analysis of the observed binding profiles. Under high surface density conditions, protein cross-linking via binding of a bivalent ligand to two immobilized TAF1 proteins, either initially or upon rebinding, could result in anomalously slow dissociation rate constants and, consequently, overestimated binding affinities (lower K_d). As a result, we utilized lower protein concentrations and shorter contact times to generate low protein density surfaces that ideally prevent the binding of bivalent ligands to more than one TAF1 protein, while maintaining a sufficiently high assay sensitivity. These SPR experiments were performed with wild-type, N1460D (**BD1** mutant) and N1583D (**BD2** mutant) TAF1, and in each case the protein density was reduced to levels allowing a maximum observed binding response of 10–25 RU. Not surprisingly, unwanted dimerization (intermolecular cross-linking) and reassociation with surface TAF1 effects were not completely abrogated at these concentrations, but manifested themselves as a component of a biphasic dissociation curve (Figure 4c). Fitting of the kinetic titrations to a heterogeneous ligand binding model allowed for discrimination of the fast and slow kinetic components (SI Table S3), where the fast kinetic components were interpreted to be representative of the bivalent *rebinding* effect, while the slow dissociation kinetics were attributed to intermolecular cross-linking and hopping. This interpretation is supported by the observation that the fast component of the kinetics accounted for the majority of the overall binding response and became predominant as the injected concentration of analyte increased, which is consistent with the hypothesis that as protein binding sites become increasingly occupied, adjacent sites are less available

to facilitate cross-linking. Additionally, the slow kinetic components of the bivalent interactions with wildtype TAF1 and the TAF1-N1460D mutant, where only the higher affinity **BD2** site is available for binding, compared favorably with affinities obtained by ITC where dimerization of TAF1 was shown to be prevalent by SEC-MALS (SI Table S3), further suggesting that the slow SPR kinetic components are a minority contribution from intermolecular cross-linking.

Kinetics-based discrimination of the intramolecular interaction event allowed for assessment of the effect of linker length on the binding affinity of the small molecules to the TAF1 protein variants (Table 1 or SI Table S3). As expected, all ligands showed similar affinities to mutant proteins TAF1-N1460D (100–200 nM) and TAF1-N1583D (≥300 nM). Interestingly, the bivalent ligands (**2**–**4**) demonstrated no substantial improvement in affinity over monovalent compound **5** for TAF1-WT protein (Table 1). Kinetic analysis was also performed at 15 °C in order to slow the kinetics of the interactions (SI Table S4); however, similar trends in kinetics and affinity were observed at 25 and 15 °C for all ligands, suggesting no substantial differences in affinities between bivalent compounds with varying linker lengths.

Based on the kinetics observed in the SPR experiments, it would appear that the bivalent ligands readily interact with TAF1-**BD2**, but show only weak evidence of simultaneous interaction with **BD1** and **BD2**. It is also possible, however, that the dissociation kinetics of the low affinity site are too fast to for a complex in which **BD1** and **BD2** are simultaneously occupied to be observable under the conditions utilized in this study. Moreover, the flow-based nature of the SPR technique makes it relatively insensitive to the bivalent *rebinding* effect, the primary driver of affinity gain when formation of high stoichiometry complexes are precluded by experimental conditions (low protein density or concentration). Indeed, quick rebinding occurs due to an elevated local concentration of the tethered ligand monomer in the vicinity of the unoccupied protein binding site according to

$$P(N, \mathbf{R}) \sim \left(\frac{3}{2\pi N l^2}\right)^{3/2} \mathrm{e}^{-3R^2/2Nl^2} \quad (2)$$

where N is the chain length in persistence length (l) units, **R** is a coordinate vector of the available binding site, and R is the distance between the protein binding sites. In SPR, during the dissociation phase of the assay, proteins and ligands are in a stationary force field due to the flow. The minimum of potential energy for the unbound tethered monomer lies on the intersection of the sphere surface delimiting the volume accessible to the unbound monomer and a plane perpendicular to the flow (Figure 4d). Potential energy of the monomer in the binding site would be equivalent to the work $\mathbf{F}d$ required to move the monomer over the distance d against the flow, where **F** is the force applied by the flow, d is the distance between the virtual plane perpendicular to the flow and tangential to the sphere accessible to the unbound ligand monomer (as depicted in Figure 4d), k is the Boltzmann constant, and T is temperature. Then, the probability for the monomer to reach the pocket due to thermal fluctuation would follow the Boltzmann distribution ($\exp(-\mathbf{F}d/kT)$). The

combined probability for the tethered monomer to reach the available pocket against the flow would be given as

$$P'(N, \mathbf{R}) \sim P(n, \mathbf{R}) e^{-\mathbf{F}d/kT} \quad (3)$$

Overall, while these SPR experiments provided a thought-provoking data set examining bivalent binding, this evidence came with its own inherent limitations due to the impact of flow to diminish *rebinding*.

Although, here and above, we identified and discussed sound qualitative rationale for the uncertainties arising from our ITC and SPR studies (which also explain apparent discrepancies between the two techniques), we still lack definitive microscopic details of how bivalent ligands **2**–**4** bind to a bivalent protein across a variety of concentration regimes. Significantly, in the context of multivalent probe utility, none of these *in vitro* techniques provide definitive insight into likely binding modes and affinity enhancement at cellular TAF1 concentrations.

Computational Deconvolution of Protein–Ligand Binding Rates and Free Energies

Due to the complexities and notable limitations of the experimental approaches described above and to gain additional microscopic insights into the kinetics of protein–ligand interactions and stationary probability densities for the resulting complexes, we employed explicit particle-based, decasecond-scale computational simulations of TAF1 and BSP-based ligands in implicit solvent. In our simulations, ligand and protein particles diffuse, under force-field constraints, in a cubic box at varying concentrations. The force field includes a physics-based component responsible for particle motions and a knowledge-based component responsible for association and dissociation events (Figure 5a). Each bivalent ligand or bivalent TAF1 protein was modeled as two spherical particles connected by a Gaussian linker (Figure 5b). Rate constants for binding of an individual monomeric BSP to **BD1** and **BD2** were fitted so that the resulting K_d would match our ITC data for **5**. Accordingly, monomeric compound **5** binds to **BD2** with $K_d \approx 700$ nM and to **BD1** with $K_d \approx 18$ μM. Diffusion coefficients for individual particles were adopted from published data.[34,35] Two ligand concentrations were used to represent the initial and final conditions of our ITC experiments (approximately 2 μM and 20 μM, respectively), while the TAF1 concentration was held constant at 26.8 μM (Figure 5c, left). For comparison, we also modeled a condition (0.01 μM ligand and 0.01 μM TAF1) that more closely recapitulates the significantly lower concentrations expected in live cells (Figure 5c, right). Indeed, recent proteomic studies show that typical protein concentrations lie in the range 10–100 nM.[36,37] However, it is worth mentioning that sometimes relatively high local concentrations might be achieved though effects of compartmentalization, scaffolding, and recruitment to regulatory epigenetic complexes or DNA.[38,39]

We then investigated the details of bivalent binding to TAF1 for ligands **2**–**4**. Apparent affinities were calculated as $K_d^{app} = \frac{[L][P]}{\sum_{i,j,k}[(L_iP_j)^{(k)}]}$, where $[L]$ and $[P]$ are the concentrations

of free ligand and free protein, respectively, and $[(L_iP_j)^{(k)}]$ is the concentration of a complex with protein–ligand stoichiometry *i:j* and valency *k*. A gain in apparent affinity, though to a different degree, was observed for all ligands under all concentrations (Table 2), and two clear trends emerged. First, there is an anticipated decrease in the apparent affinity with an increase of the linker length under cellular concentration conditions (but not under ITC concentration conditions). Second, and less expected, there is a significant decrease in the binding affinity of each bivalent ligand with a decrease in the protein concentration.

Similar to the experimental results described above, our simulations reinforce the intricacies of multiple competing processes in multivalent interactions. In particular, in simulations under cellular-like concentration conditions, virtually no protein:ligand complexes with 1:2 stoichiometry were observed. Consequently, the apparent affinity was dominated by the intramolecular, linker-dependent *rebinding* effect, where 80–90% of 1:1 complexes featured bivalent protein–ligand interactions (Figure 1c). Accordingly, the apparent affinity calculated under cellular conditions for compound **2**, featuring the PEG_4 linker (K_d = 19 nM), was more than 8-fold higher than that for compound **4**, featuring the PEG_{29} linker (K_d = 164 nM). In contrast, under ITC-like concentration conditions, 2:1 protein:ligand complexes represented the dominant species. As a result, the apparent affinity was subject to two competing trends: (i) bivalent *rebinding*, decreases with increasing linker lengths, and (ii) binding of two proteins by a single ligand, increases with increasing protein concentration. Consequently, bound ligand **4** having a significantly longer linker than **2** (PEG_{29} vs PEG_4) spends a significantly longer time with one BSP monomeric unit unbound because a longer search time is required to reach the second binding site. This contributes to an overall shorter residence time on a single protein, but makes its unbound unit available for binding by another protein in a 2:1 protein:ligand complex.

In addition, we investigated which of the theoretically possible complexes (Figure 1) were actually observed in our simulations and determined their respective dissociation microconstants. Microconstants were calculated as $K_d^{ijk} = \frac{[L][P]}{[(L_iP_j)^{(k)}]}$, where $[(L_iP_j)^{(k)}]$ is the concentration of the protein–ligand complex $(L_iP_j)^{(k)}$, and $[L]$ and $[P]$ are, respectively, concentrations of ligand and protein not involved in $(L_iP_j)^{(k)}$. Three types of complexes were detected in all simulations: 1:1 monovalent (Figure 1a), 1:1 bivalent (Figure 1c,d) and 1:2 (Figure 1e) protein:ligand complexes. Similar to the apparent K_d values, dissociation microconstants showed significant dependence on the linker length and concentration conditions (Table 2). Under ITC concentration conditions, 2:1 protein:ligand complexes are dominant and make up 70% (compound **2**) to 93% (compound **4**) of the ligand bound complexes. This dominant population of TAF1 dimers is consistent with our SEC-MALS data (Figure 4b). Also, in the simulations that mimic ITC conditions, the population of bivalently bound 1:1 complexes (Figure 1c) largely decreases as linker length increases (87% (**2**) to 55% (**3**) to 28% (**4**)).

CONCLUSIONS

In this study, a series of bivalent ligands based on the pan active bromodomain inhibitor, BSP, were designed and synthesized for the dual-bromodomain module of TAF1 as a model

system for the investigation of multivalent binding interactions with the potential benefit of increased potency and selectivity relative to the corresponding monovalent interactions. Utilizing various experimental techniques including ITC, SEC, and SPR, we set out to systematically demonstrate that the bivalent ligands were potent TAF1 inhibitors, potent inhibition was driven by the anticipated mode of multivalent binding, and the appropriate linker length was key for enabling multivalent interactions. Encouragingly, bivalent compounds **2**, **3**, and **4** demonstrated potent TAF1 binding and provided a significant affinity gain with respect to the corresponding monovalent ligand as determined by ITC. However, when considering the physical details underlying each approach, we were struck by the complexities and challenges associated with evaluating multivalent binding interactions in each of these *in vitro* systems, many of which limit simplistic interpretations, yet are commonly overlooked in other studies. Based on our studies, ITC appears to overestimate the apparent K_d for multivalent ligands by almost an order of magnitude due to the significant presence of high-stoichiometry complexes resulting from the high protein concentrations required. Furthermore, SPR is less sensitive to the entropic 1:1 *rebinding* effect, which is so critical for effective multivalent binding, due to the effect of solvent flow on the accessibility of binding sites. Importantly, these biophysical and structural studies provided valuable input for subsequent computational simulations that could assess the entropy-dominated *rebinding* affinities of our ligands under various concentration conditions, including those characteristics of live cells. Moving forward, such computational approaches are likely to be effective in the design and evaluation of potent bivalent ligands for multidomain proteins, circumventing the complexities of correlating experimental affinity enhancements observed across assay types and concentration regimes. Ultimately, the utility of bivalent ligands over their monovalent counterparts will go undisputed when demonstrated in the context of a cellular system, and encouragingly, there are numerous examples which reveal the effectiveness of bivalent target engagement in cells.[10,11,40] Initial cellular studies with these TAF1 multivalent ligands suggest that improvements in cellular penetration will be needed to test this hypothesis further.

Supplementary Material

Refer to Web version on PubMed Central for supplementary material.

Acknowledgments

Funding

This work was supported by the National Institute of General Medical Sciences, U.S. National Institutes of Health (NIH) (Grant R01GM100919) to S.V.F., by the UNC Eshelman Institute for Innovation (Grants RX0351210 and RX03712105) to D.B.K. and a Kwanjeong Educational Foundation award (13AmB65D) to J.L.S.

The authors thank Ken Pearce and Frances Potjewyd for reviewing the primary data supporting this manuscript. We acknowledge Ashutosh Tripathy, director of the UNC Macro-molecular Interactions Facility, for assistance with ITC, SEC-MALS and CD experiments.

References

1. Fasting C, Schalley CA, Weber M, Seitz O, Hecht S, Koksch B, Dernedde J, Graf C, Knapp EW, Haag R. Multivalency as a Chemical Organization and Action Principle. Angew Chem, Int Ed. 2012; 51:10472–10498.

2. Mulder A, Huskens J, Reinhoudt DN. Multivalency in supramolecular chemistry and nanofabrication. Org Biomol Chem. 2004; 2:3409–3424. [PubMed: 15565230]
3. Kiessling LL, Gestwicki JE, Strong LE. Synthetic multivalent ligands as probes of signal transduction. Angew Chem, Int Ed. 2006; 45:2348–2368.
4. Mammen M, Choi SK, Whitesides GM. Polyvalent interactions in biological systems: Implications for design and use of multivalent ligands and inhibitors. Angew Chem, Int Ed. 1998; 37:2755–2794.
5. Frye SV. The art of the chemical probe. Nat Chem Biol. 2010; 6:159–161. [PubMed: 20154659]
6. Bunnage ME, Chekler ELP, Jones LH. Target validation using chemical probes. Nat Chem Biol. 2013; 9:195–199. [PubMed: 23508172]
7. Illendula A, Pulikkan JA, Zong H, Grembecka J, Xue L, Sen S, Zhou Y, Boulton A, Kuntimaddi A, Gao Y, Rajewski RA, Guzman ML, Castilla LH, Bushweller JH. Chemical biology. A small-molecule inhibitor of the aberrant transcription factor CBFbeta-SMMHC delays leukemia in mice. Science. 2015; 347:779–784. [PubMed: 25678665]
8. Arrowsmith CH, Bountra C, Fish PV, Lee K, Schapira M. Epigenetic protein families: a new frontier for drug discovery. Nat Rev Drug Discovery. 2012; 11:384–400. [PubMed: 22498752]
9. Ruthenburg AJ, Li H, Patel DJ, Allis CD. Multivalent engagement of chromatin modifications by linked binding modules. Nat Rev Mol Cell Biol. 2007; 8:983–994. [PubMed: 18037899]
10. Tanaka M, Roberts JM, Seo HS, Souza A, Paulk J, Scott TG, DeAngelo SL, Dhe-Paganon S, Bradner JE. Design and characterization of bivalent BET inhibitors. Nat Chem Biol. 2016; 12:1089–1096. [PubMed: 27775715]
11. Rhyasen GW, Hattersley MM, Yao Y, Dulak A, Wang W, Petteruti P, Dale IL, Boiko S, Cheung T, Zhang J, Wen S, Castriotta L, Lawson D, Collins M, Bao L, Ahdesmaki MJ, Walker G, O'Connor G, Yeh TC, Rabow AA, Dry JR, Reimer C, Lyne P, Mills GB, Fawell SE, Waring MJ, Zinda M, Clark E, Chen H. AZD5153: A Novel Bivalent BET Bromodomain Inhibitor Highly Active against Hematologic Malignancies. Mol Cancer Ther. 2016; 15:2563–2574. [PubMed: 27573426]
12. Wassarman DA, Sauer F. TAF(II)250: a transcription toolbox. Journal of Cell Science. 2001; 114:2895–2902. [PubMed: 11686293]
13. Jacobson RH, Ladurner AG, King DS, Tjian R. Structure and function of a human TAFII250 double bromodomain module. Science. 2000; 288:1422–1425. [PubMed: 10827952]
14. Picaud S, Leonards K, Lambert JP, Dovey O, Wells C, Fedorov O, Monteiro O, Fujisawa T, Wang CY, Lingard H, Tallant C, Nikbin N, Guetzoyan L, Ingham R, Ley SV, Brennan P, Muller S, Samsonova A, Gingras AC, Schwaller J, Vassiliou G, Knapp S, Filippakopoulos P. Promiscuous targeting of bromodomains by bromosporine identifies BET proteins as master regulators of primary transcription response in leukemia. Sci Adv. 2016; 2:e1600760. [PubMed: 27757418]
15. Diestler DJ, Knapp EW. Statistical Thermodynamics of the Stability of Multivalent Ligand-Receptor Complexes. Phys Rev Lett. 2008; 100:178101. [PubMed: 18518340]
16. Karush, F. Contemporary Topics in Molecular Immunology. Springer; 1976. Multivalent binding and functional affinity; p. 217-228.
17. Kitov PI, Bundle DR. On the nature of the multivalency effect: a thermodynamic model. J Am Chem Soc. 2003; 125:16271–16284. [PubMed: 14692768]
18. Jencks WP. On the attribution and additivity of binding energies. Proc Natl Acad Sci U S A. 1981; 78:4046–4050. [PubMed: 16593049]
19. Pronk S, Páll S, Schulz R, Larsson P, Bjelkmar P, Apostolov R, Shirts MR, Smith JC, Kasson PM, van der Spoel D. GROMACS 4.5: a high-throughput and highly parallel open source molecular simulation toolkit. Bioinformatics. 2013; 29:845–854. [PubMed: 23407358]
20. Vanommeslaeghe K, Hatcher E, Acharya C, Kundu S, Zhong S, Shim J, Darian E, Guvench O, Lopes P, Vorobyov I, Mackerell AD. CHARMM general force field: A force field for drug-like molecules compatible with the CHARMM all-atom additive biological force fields. J Comput Chem. 2009; 31:671–690.
21. Zoete V, Cuendet MA, Grosdidier A, Michielin O. SwissParam: A fast force field generation tool for small organic molecules. J Comput Chem. 2011; 32:2359–2368. [PubMed: 21541964]
22. Mark P, Nilsson L. Structure and Dynamics of the TIP3P, SPC, and SPC/E Water Models at 298 K. J Phys Chem A. 2001; 105:9954–9960.

23. Hess B, Bekker H, Berendsen HJ, Fraaije JG. LINCS: a linear constraint solver for molecular simulations. J Comput Chem. 1997; 18:1463–1472.
24. Essmann U, Perera L, Berkowitz M, Darden T, Lee H, Pedersen L. A smooth particle mesh Ewald method. J Chem Phys. 1995; 103:8577–8593.
25. Berendsen HJ, Postma Jv, van Gunsteren WF, DiNola A, Haak J. Molecular dynamics with coupling to an external bath. J Chem Phys. 1984; 81:3684–3690.
26. Northrup SH, Allison SA, McCammon JA. Brownian dynamics simulation of diffusion-influenced bimolecular reactions. J Chem Phys. 1984; 80:1517–1524.
27. Chow E, Skolnick J. Effects of confinement on models of intracellular macromolecular dynamics. Proc Natl Acad Sci U S A. 2015; 112:14846–14851. [PubMed: 26627239]
28. Young M, Carroad P, Bell R. Estimation of diffusion coefficients of proteins. Biotechnol Bioeng. 1980; 22:947–955.
29. Zhu J, Caflisch A. Twenty Crystal Structures of Bromodomain and PHD Finger Containing Protein 1 (BRPF1)/ Ligand Complexes Reveal Conserved Binding Motifs and Rare Interactions. J Med Chem. 2016; 59:5555–5561. [PubMed: 27167503]
30. Li AG, Piluso LG, Cai X, Gadd BJ, Ladurner AG, Liu X. An acetylation switch in p53 mediates holo-TFIID recruitment. Mol Cell. 2007; 28:408–421. [PubMed: 17996705]
31. Lee H, Venable RM, Mackerell AD Jr, Pastor RW. Molecular dynamics studies of polyethylene oxide and polyethylene glycol: hydrodynamic radius and shape anisotropy. Biophys J. 2008; 95:1590–1599. [PubMed: 18456821]
32. Filippakopoulos P, Picaud S, Mangos M, Keates T, Lambert JP, Barsyte-Lovejoy D, Felletar I, Volkmer R, Muller S, Pawson T, Gingras AC, Arrowsmith CH, Knapp S. Histone recognition and large-scale structural analysis of the human bromodomain family. Cell. 2012; 149:214–231. [PubMed: 22464331]
33. Tarazona MP, Saiz E. Combination of SEC/ MALS experimental procedures and theoretical analysis for studying the solution properties of macromolecules. J Biochem Biophys Methods. 2003; 56:95–116. [PubMed: 12834971]
34. Verkman AS. Solute and macromolecule diffusion in cellular aqueous compartments. Trends Biochem Sci. 2002; 27:27–33. [PubMed: 11796221]
35. Young ME, Carroad PA, Bell RL. Estimation of Diffusion-Coefficients of Proteins. Biotechnol Bioeng. 1980; 22:947–955.
36. Wiśniewski JR, Hein MY, Cox J, Mann M. A “proteomic ruler” for protein copy number and concentration estimation without spike-in standards. Mol Cell Proteomics. 2014; 13:3497–3506. [PubMed: 25225357]
37. Liu Y, Beyer A, Aebersold R. On the dependency of cellular protein levels on mRNA abundance. Cell. 2016; 165:535–550. [PubMed: 27104977]
38. Aguzzi A, Altmeyer M. Phase separation: linking cellular compartmentalization to disease. Trends Cell Biol. 2016; 26:547–558. [PubMed: 27051975]
39. Good MC, Zalatan JG, Lim WA. Scaffold proteins: hubs for controlling the flow of cellular information. Science. 2011; 332:680–686. [PubMed: 21551057]
40. Waring MJ, Chen H, Rabow AA, Walker G, Bobby R, Boiko S, Bradbury RH, Callis R, Clark E, Dale I, Daniels DL, Dulak A, Flavell L, Holdgate G, Jowitt TA, Kikhney A, McAlister M, Mendez J, Ogg D, Patel J, Petteruti P, Robb GR, Robers MB, Saif S, Stratton N, Svergun DI, Wang W, Whittaker D, Wilson DM, Yao Y. Potent and selective bivalent inhibitors of BET bromodomains. Nat Chem Biol. 2016; 12:1097–1104. [PubMed: 27775716]

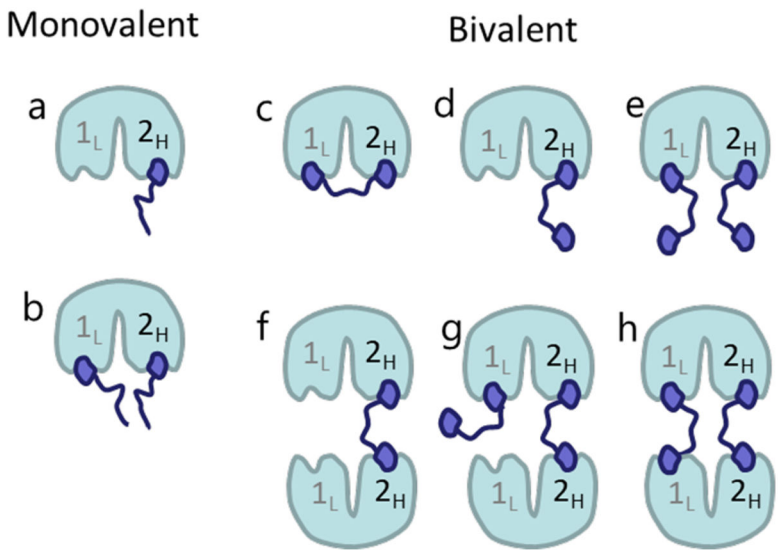

Figure 1.

High probability protein–ligand complexes that can be formed by TAF1 with BSP-based monovalent (a,b) and bivalent (c–h) ligand. (1_L: low affinity binding site (BD1); 2_H: high affinity binding site (BD2)).

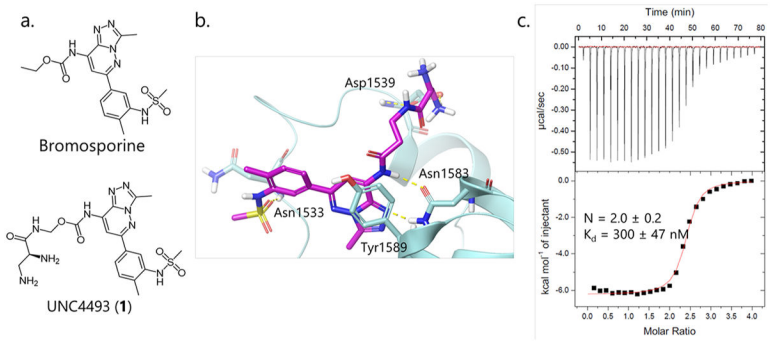

Figure 2.

(A) Chemical structures of BSP and UNC4493 (**1**). (B) A model of UNC4493 (**1**) in complex with TAF1 **BD2**. (C) ITC results for UNC4493 (**1**) binding to TAF1 **BD1**-**BD2**.

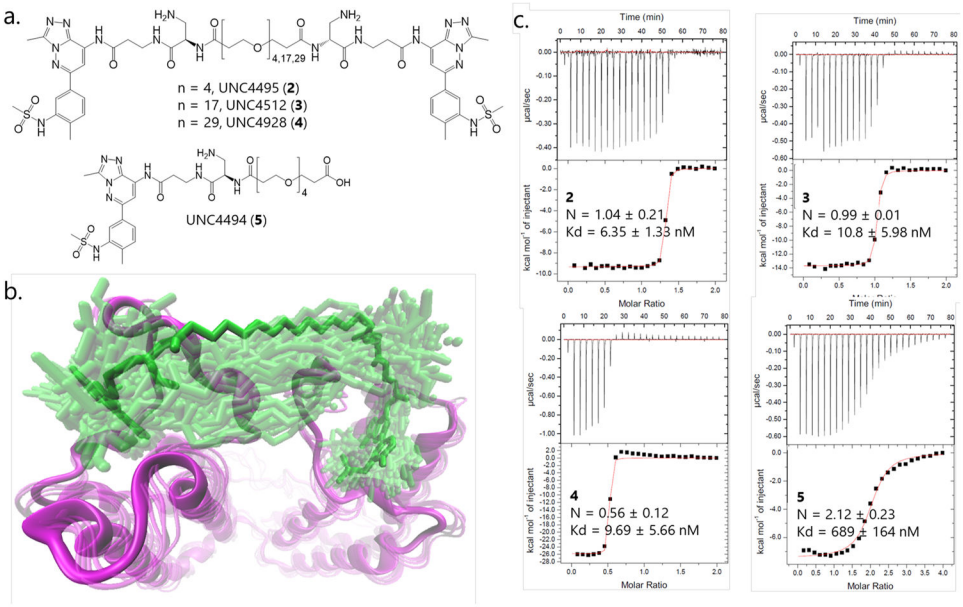

Figure 3.

(A) Structures of bivalent PEG-linked BSP compounds (**2**–**4**) and the monovalent PEG-linked reference compound (**5**). (B) Snapshots from the MD trajectory of compound **2** (green sticks) in complex with TAF1 **BD1**–**BD2** (magenta ribbons) (the initial docking model shown in solid sticks/ribbon, other frames in transparent sticks/ribbon). (C) ITC results for compounds **2**–**5** with TAF1 **BD1**–**BD2**.

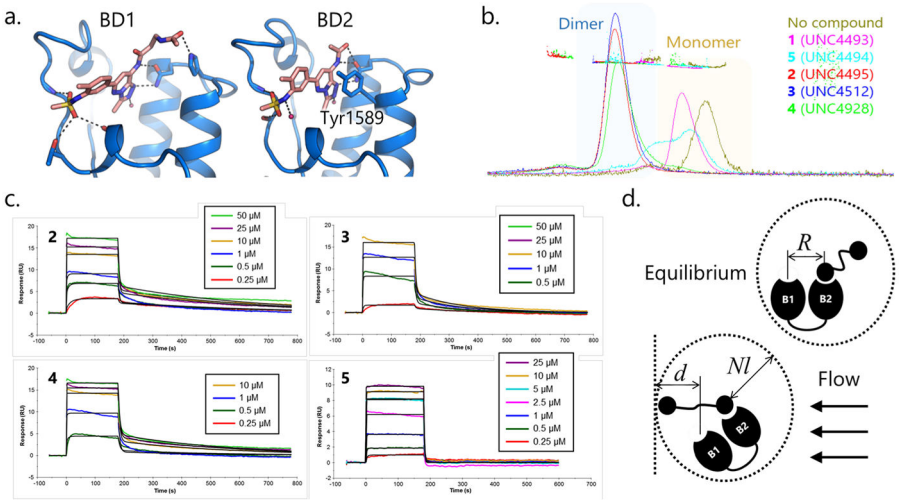

Figure 4.

(A) Co-crystal structure of TAF1 **BD1**–**BD2** (blue) in complex with compound **3** (orange). (B) SEC-MALS data with TAF1 **BD1**–**BD2** and various BSP based ligands. (C) SPR kinetic titration binding profiles for wild-type TAF1 **BD1**–**BD2** with compounds **2**–**5**. (D) Schematic depicting the geometry of the bivalent rebinding effect under equilibrium and SPR flow conditions.

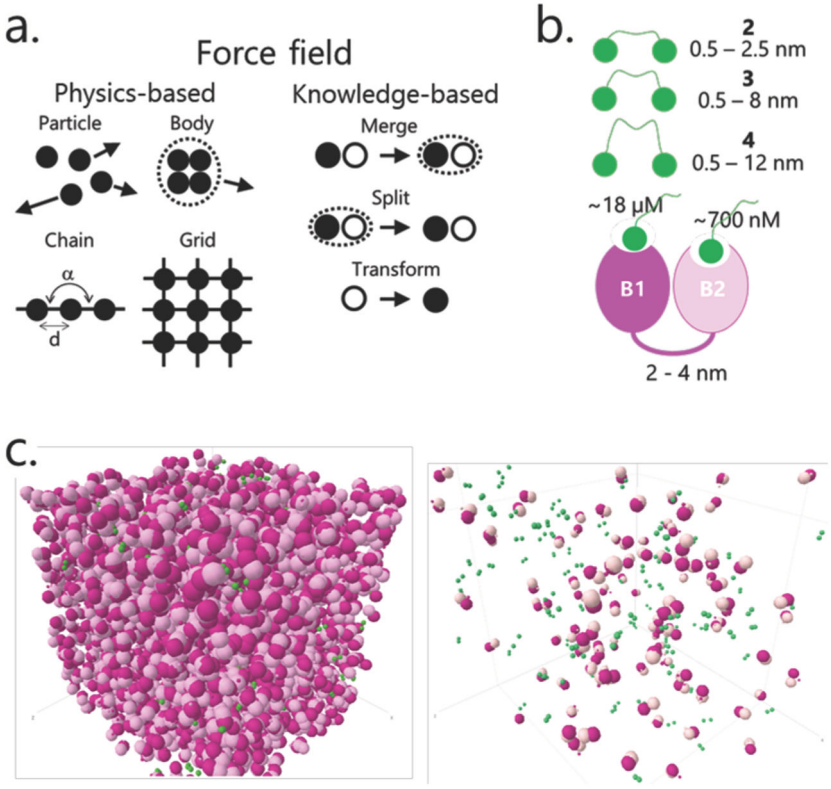

Figure 5.

(A) Basic components of the particle-based simulation approach used. (B) Physical parameters of ligand (green) and protein (pink) models used in simulations. (C) Visual snapshots from simulations in ITC (left) and cellular (right) concentration conditions.

Table 1

Association and Dissociation Rate Constants (k_a, k_d) and Apparent Affinity Constants (K_d) for Binding of Ligands 2–5 with Wild-Type TAF1 and TAF1 N1460D and N1583D Mutants as Measured by SPR[a]

N1460D	**k_a(×10^6 M^{-1} s^{-1})**	**k_d (×10^{-1} s^{-1})**	**K_d (nM)**
2	1.6 ± 0.1	1.7 ± 0.2	110 ± 10
3	1.1 ± 0.2	2.5 ± 0.1	230 ± 40
4	1.5 ± 0.1	3.6 ± 0.5	230 ± 40
5	1.8 ± 0.2	3.3 ± 0.1	190 ± 30
N1583D	k_a (×10^6 M^{-1} s^{-1})	k_d (×10^{-1} s^{-1})	K_d (nM)
2	0.8 ± 0.1	5 ± 1	600 ± 200
3	0.9 ± 0.4	≥10 ± ND	≥1000 ± ND
4	3.2 ± 0.7	≥10 ± ND	≥300 ± ND
5	0.2 ± 0.0	5 ± 2	3000 ± 1000
WT	k_a (×10^6 M^{-1} s^{-1})	k_d (×10^{-1} s^{-1})	K_d (nM)
2	2.0 ± 0.3	3.4 ± 0.4	170 ± 30
3	1.4 ± 0.4	1.9 ± 10.1	140 ± 40
4	2.8 ± 0.6	2.2 ± 0.2	80 ± 20
5	2.1 ± 0.4	4.6 ± 0.8	220 ± 50

[a]All values represent the averages and standard (k_a, k_d) and propagated (K_d) errors from replicate measurements obtained at 25 °C. Interactions with dissociation rates (k_d) ≥ 1 s^{-1} were rounded to 1 s^{-1}, the limit of detection for the instrument, apparent affinities were calculated accordingly, and errors were not determined (ND).

Table 2

Experimental (ITC and SPR) and Calculated Apparent Affinity Constants (K_d) of the Interaction of TAF1-WT with the Monovalent Ligand 5 and Bivalent Ligands 2–4 under Varying Concentration Conditions, and Respective Calculated Dissociation Microconstants for 1:1 and 2:1 Protein–Ligand Complexes[a]

			2038/26 818 ([L]/[P])			18 562/24 424			100/100		
ligand	K_d^{ITC} (nM)	K_d^{SPR} (nM)	K_d^{app}	$K_d^{1:1}$	$K_d^{2:1}$	K_d^{app}	$K_d^{1:1}$	$K_d^{2:1}$	K_d^{app}	$K_d^{1:1}$	$K_d^{2:1}$
2	6.4 ± 1.3	170 ± 30	4.8 ± 1.9	7490	87 550	14 ± 1.1	391	41 800	19 ± 0.2	19	∞
3	10.8 ± 6.0	140 ± 40	25 ± 12	54 064	11 767	50 ± 2.2	2584	73 528	77 ± 6.8	78	>100 000
4	9.7 ± 5.7	80 ± 20	18 ± 12	15 500	4230	50 ± 4.5	7145	28 159	164 ± 7.2	172	24 714
5	689 ± 164	220 ± 50	700 ± 14	700 ± 14	-	705 ± 18	705 ± 18	-	730 ± 27	730 ± 27	-

[a]All values represent the averages and standard errors from replicate measurements and simulations. Concentrations are expressed in nM. $K_d^{1:1}$ is the dissociation microconstant for complexes interacting with 1:1 stoichiometry (both monovalent and bivalent), $K_d^{2:1}$ is dissociation microconstant for 2:1 protein–ligand complexes.